A Review on Recent Developments in Fully Polarimetric SAR Image Despeckling

Xiaoshuang Ma, Penghai Wu, *Member, IEEE*, Yanlan Wu, and Huanfeng Shen, *Senior Member, IEEE*

***Abstract*—The use of synthetic aperture radar (SAR) technology with quad-polarization data requires efficient polarimetric SAR (PolSAR) speckle filtering algorithms. During the last three decades, many effective methods have been developed to reduce the speckle in PolSAR images, and recent studies have generally shown a trend developing from local single-point filtering to nonlocal patch-based or globally collaborative filtering. The main goals of this paper are to make a comprehensive review of the existing PolSAR despeckling algorithms and highlight the recent development trends. In the experimental part, the filtering results obtained with both simulated and real PolSAR images are deployed to compare the performance of some of the state-of-the-art despeckling algorithms, which shows that all of the selected filters have their individual strengths and weaknesses.**

***Index Terms*—Nonlocal means (NLM), polarimetric synthetic aperture radar (PolSAR), speckle filtering, Wishart distribution.**

I. Introduction

SYNTHETIC aperture radar (SAR) systems have the capability to capture images of the earth in both day and night, and for almost all weather conditions. Polarimetric SAR (PolSAR) is an advanced form of SAR,which focuses on emitting and receiving fully polarized radar waves to characterize observed targets. Compared with optical remote sensing data, PolSAR data have unique advantages in obtaining land-cover information, which has resulted in their wide use in many areas. However, SAR data are inherently affected by speckle noise. The presence of speckle complicates the image interpretation and land surface parameter inversion. Compared with single-polarization SAR data, the speckle model of fully PolSAR data is much more complicated. Speckle noise not only appears in the intensity image of each polarization, but also in the complex cross-product terms [1].

In most of the cases, despeckling is an essential procedure before using SAR images to obtain land-cover information. As described in Section III, many different methods have been proposed to reduce the speckle of PolSAR images and have generally shown positive performances. It should be pointed out that a good review of PolSAR filtering methods has been written by Foucher and López-Martínez [2]. However, the main objective of the work in [2] was to perform an analysis and a comparison of some of the traditional and classical PolSAR filters. In recent years, PolSAR image filtering has shown a rapid development trend. In particular, a number of despeckling methods based on the ideas of nonlocal means (NLM) and total variation (TV) have been proposed and have shown good performances, and these methods were not included in [2]. In general, the recent developments of PolSAR filtering methods have shown the trend evolving from local single-point processing to nonlocal patch-based or globally collaborative filtering. Therefore, a comprehensive review of the existing PolSAR filtering algorithms from the new viewpoint is required, which is the main goal of this paper.

The remainder of this paper is organized as follows. Section II recalls the statistical models of PolSAR data. A comprehensive review of the existing despeckling methods is made in Section III, and some of the quantitative assessment indexes are introduced in Section IV. Then, in Section V, we describe the experiments conducted on both simulated and real PolSAR images to compare the performance of some of the state-of-the-art despeckling algorithms. Finally, the conclusions are provided in Section VI.

II. Statistical Models of PolSAR Data

A polarimetric radar system measures the complex scattering matrix of a medium with quad-polarizations. Single-look PolSAR data can be characterized by a complex scattering matrix

$$\mathbf{S} = \begin{bmatrix} S_{HH} & S_{HV} \\ S_{VH} & S_{VV} \end{bmatrix} \tag{1}$$

where S_{HV} denotes the scattering element of the horizontal transmitting and vertical receiving polarizations, with the combination of the amplitude $|S_{HV}|$ and the phase ϕ_{HV}: $S_{HV} = |S_{HV}|e^{j\phi_{HV}}$. The other elements in the scattering matrix are similarly defined. For the reciprocal backscattering case, $S_{HV} = S_{VH}$. Single-look polarimetric data can also be represented by a polarimetric covariance matrix, which is generated from the outer product of the target vector with its conjugate transpose. SAR data are frequently multilook processed for

Manuscript received July 8, 2017; revised September 26, 2017; accepted October 25, 2017. Date of publication November 9, 2017; date of current version March 9, 2018. This work was supported by the National Natural Science Foundation of China under Grant 41271376 and Grant 61671334, the Natural Science Foundation of the Department of Education of Anhui Province (KJ2017A037), and by the Start-up Foundation for Doctoral Research of Anhui University (J01003226). *(Corresponding authors: Penghai Wu and Huanfeng Shen.)*

X. Ma, P. Wu, and Y. Wu are with the Department of Resources and Environmental Engineering, Anhui University, Hefei 230000, China (e-mail: mxs.88@whu.edu.cn; wuph@ahu.edu.cn; wylmq@sohu.com).

H. Shen is with the Department of Resource and Environmental Sciences, Wuhan University, Wuhan 430072, China (e-mail: shenhf@whu.edu.cn).

Color versions of one or more of the figures in this paper are available online at http://ieeexplore.ieee.org.

Digital Object Identifier 10.1109/JSTARS.2017.2768059

speckle reduction and data compression by averaging several neighboring single-look pixels.

Most of the PolSAR filters were derived based on the assumption of "fully developed speckle," which has the following properties [3]:

1) a large number of scatterers in a resolution cell of a homogeneous medium;
2) the range distance is much larger than the radar wavelength;
3) the surface is much rougher than the scale of the radar wavelength.

It has been proven that, for fully developed speckle, the L-look covariance matrix $\mathbf{C}_L$ follows a complex Wishart distribution [4]:

$$P(\mathbf{C}_L|\mathbf{Z}) = \frac{L^{qL}|\mathbf{C}_L|^{L-q}\exp\{-LTr(\mathbf{Z}^{-1}\mathbf{C}_L)\}}{Q(L,q)|\mathbf{Z}|^L} \quad (2)$$

with

$$Q(L,q) = \pi^{q(q-1)/2}\prod_{i=1}^{q}\Gamma(L-i+1) \quad (3)$$

where $Tr(\cdot)$ and $|\cdot|$ are, respectively, the trace operator and the determinant operator. $\mathbf{Z}$ is the population covariance matrix. The parameter $q = 3$ is the dimension of the polarimetric covariance matrix.

The complex Wishart distributions were derived to model pure fully developed speckle, which is a zero-mean complex circular Gaussian process. In the presence of spatial texture, such as urban and forest areas in images with a high resolution, the circular Gaussian assumption is no longer valid. To account for the texture effect in polarimetric SAR images, some other statistical models have been proposed. Beyond these models, the K-distribution [5] is particularly attractive. The PDF of the K-distributed polarimetric covariance matrix $\mathbf{C}_L$ is given by

$$P_K(\mathbf{C}_L|\mathbf{Z}) = \frac{2|\mathbf{C}_L|^{L-q}(L\alpha)^{(\alpha+qL)/2}}{Q(L,q)|\mathbf{Z}|^L\Gamma(\alpha)} \times \frac{K_{\alpha-qL}(2\sqrt{L\alpha Tr(\mathbf{Z}^{-1}\mathbf{C}_L)})}{Tr(\mathbf{Z}^{-1}\mathbf{C}_L)^{-(\alpha-qL)/2}} \quad (4)$$

where $K_{\alpha-qL}(\cdot)$ is the modified Bessel function of the second kind, with the order $\alpha - qL$. Parameter α depicts the homogeneity of the scene.

III. PolSAR Speckle Filtering

A. PolSAR Despeckling Principles

It is well known that the speckle in single-channel SAR data (intensity or amplitude) can be modeled as multiplicative noise. However, the speckle model of fully PolSAR data is much more complicated. The speckle noise associated with the diagonal terms of the covariance or coherency matrix is multiplicative in nature, but the off-diagonal terms are a combination of additive and multiplicative natures, depending on the magnitude of the correlation coefficient between the two polarizations [1]. The works by Lee *et al*. [9] and López-Martínez and Fabregas [17] specified the general principles of a PolSAR speckle filter.

An agreement of the conclusions in [9] and [17] is that the information that needs to be retrieved for PolSAR filtering is of the second-order moments of the multidimensional SAR data [2]. The authors of [9] and [17] proposed the use of polarimetric covariance or coherency matrices. That is to say, they assumed that these matrices contain all the necessary information to characterize PolSAR data. Of course, this assumption is only valid for the case of fully developed speckle. From the image processing viewpoint, the major difference between the filtering principles proposed in [9] and [17] is whether or not the diagonal terms and the off-diagonal terms should be filtered in the same way. In [9], the authors proposed that, to preserve the polarimetric properties, all the terms of the matrix should be filtered in the same way, i.e., filtered by the same amount. Furthermore, to avoid crosstalk between the polarization channels, each element of the covariance matrix is filtered independently in the spatial domain. To date, most of the researchers have followed these principles when developing PolSAR filters. In [17], the authors suggested that the above PolSAR filtering principles can be relaxed. Since the noise model presented in [1] indicates that the speckle in an off-diagonal term presents a complex additive and multiplicative combined nature for low coherence values, whereas speckle tends to be multiplicative in the case of high coherence, the filters that adapt to the type of noise in the off-diagonal terms can obtain better results. However, in a recent paper, Lee *et al.* [12] claimed that the use of a filter to process the terms of the matrix differently is inappropriate. They pointed out that PolSAR speckle filters should aim to preserve scattering properties, and not enhance them.

B. PolSAR Filters

The multilook method of SAR imaging processing, which, in the current SAR systems, is often accomplished by averaging the neighboring single-look pixels in the azimuth direction, can reduce the noise amount, but at the cost of a clear loss in spatial resolution. Therefore, despeckling algorithms are often necessary. The studies of PolSAR filters can be traced back to the beginning of the 1990s. Although some early techniques were developed to filter PolSAR data, they cannot be regarded as PolSAR speckle filters because the off-diagonal terms of the covariance or coherency matrix were either ignored or improperly filtered [3]. During the last three decades, many different PolSAR filtering techniques have been developed. These techniques can be generally categorized into five classes, namely, local window filters, NLM-based methods, partial differential equation (PDE)-based methods, variational methods, and machine-learning-based methods. Of course, the separation between the different classes is not strict, as some filtering techniques can be assigned to two or more classes at the same time. The objective of this part is to make a broad review of the existing PolSAR despeckling techniques, especially the typical methods proposed in recent years, but not to provide the full details of every method, as full details can be found in the relevant references.

1) Local Window Filters: Local window filters are a classical type of filtering algorithm, which usually estimate the center

pixel by the related pixels in a local window, utilizing the statistical properties of the noisy data. In early years, the most commonly applied filtering technique was the boxcar filter, which restores the center pixel in a moving window with the average of all the pixels in the window. The boxcar filter is simple to apply and effective in reducing speckle in homogeneous areas, but clearly degrades the spatial resolution of the image. Goze and Lopes [8] generalized the method proposed by Lee *et al.* [7], which uses a multiplicative noise model to filter intensity images, to include all the terms of the covariance matrix. Another early PolSAR despeckling method, the polarimetric whitening filter, was proposed by Novak and Burl [6]. However, most of these early methods have the major drawbacks of exploiting the statistical correlations between polarization channels and changing the polarimetric properties.

a) Refined Lee filter: To solve the above problems that the early algorithms encountered, J.-S. Lee has undertaken some remarkable research into PolSAR speckle reduction. In [9], Lee employed the linear minimum mean-squared error (LMMSE) estimator to filter PolSAR data, which was termed the refined Lee PolSAR filter. In this paper, Lee proposed the basic filtering principles of PolSAR data, as introduced in Section III-A. Studies have shown that ensuring stationarity of the scene helps to improve the performance of the LMMSE estimator. To select homogeneous pixels, an edge-aligned window technique is used in the refined Lee filter.

b) Other LMMSE-based methods: The refined Lee filter opened an important branch of filtering methods based on the LMMSE estimator. The core issue of these methods is to investigate means of selecting similar pixels to ensure stationarity of the scene. In [13], a method was proposed by Lee *et al.* to select similar pixels based on the same polarimetric scattering characteristics, and the selected pixels were used to filter the preprocessed pixel by the LMMSE estimator. In [14], an intensity-driven adaptive-neighborhood filter was proposed, in which the pixels were selected by a technique of region growing, based on the intensity similarity of the polarimetric coherency matrices.

c) Extended sigma filter: The original sigma filter for single-channel SAR data was introduced by Lee [10] in 1983 to select similar pixels in a local window and to then filter the center pixel by averaging these pixels. This method has been deployed for many years due to its simplicity and effectiveness in reducing speckle. However, some deficiencies have been found [12]:

1) it fails to maintain the mean value and produces biased results;
2) strong returns from point targets are blurred and their power is reduced;
3) dark spotty pixels are not filtered.

In [11], Lee *et al.* generalized the idea of the sigma filter to select similar pixels in the local window and to filter the center pixel by the LMMSE estimator, without the deficiencies of the original sigma filter in underestimating and blurring strong targets; in the meantime, the bias introduced by the original sigma range is also compensated in the improved sigma filter. More recently, Lee *et al.* [12] proposed a new algorithm to further amend the improved sigma filter and extended it to filter PolSAR data, which was termed the extended sigma filter. The main modifications of the extended sigma filter compared to the improved sigma filter consist of a more sophisticated strategy of detecting strong point targets and selecting similar pixels using more polarimetric information.

d) Bilateral filter: To avoid oversmoothing, the filtering process of most of the traditional algorithms is often limited to a small local window. The bilateral filter expands the filtering window to a larger size. The bilateral filter was first developed for digital image denoising [15] and was recently extended to the filtering of PolSAR images by D'Hondt *et al.* [16]. In the bilateral filter, the value of the pixel centered at a large square window is estimated by the weighted average of all the pixels in the window. The weights are determined by both the polarimetric similarity and the spatial distance between the sample pixels and the preprocessed pixel. It has been reported that the bilateral filter can perform better in reducing speckle than many other local filters; however, as is well known, this filter does not perform well on images with a high level of noise [51]. It should be noted that, to some extent, the bilateral filter is a predecessor of the NLM filter, which is discussed in the NLM-based method part.

Other local filters include, but are not limited to, filters based on segmentation [19] and filters based on mean shift [20], [21]. In [19], Alonso-González *et al.* proposed a PolSAR segmentation algorithm based on binary partition trees and took each segment as a whole to filter all the pixels in it. In [20] and [21], mean-shift-based PolSAR filters were proposed. The mean-shift-based filters use moving, not fixed, windows to select the homogeneous pixels, considering both the spatial and polarimetric information. A weighted average is then used to estimate the value of the central pixel.

2) NLM-Based Methods: During the last decade, benefiting from the appearance of a series of new directions in image processing, studies of image denoising have developed rapidly. Among these new theories, the NLM filter, which was originally designed for digital image denoising [28], has been successfully extended to process PolSAR images in recent years, and good results have been reported. Differing from the traditional methods, the NLM filter not only searches and compares the values in a single point in a small local window, but also the geometrical configuration in the whole image, so it can obtain more robust results. In practice, to reduce the computational burden, the search area is limited to a large window. In a sense, the NLM filter is a relatively simple generalization of the bilateral filter [51]: the two terms measuring the difference between two single points in the bilateral similarity kernel are simply replaced with a patch-based term, and the geometric distance between pixels is ignored, leading to strong contribution from patches that may not be spatially near the pixel of interest (hence the name *nonlocal*).

a) Pretest NLM: In [29], the PolSAR NLM filter with a pretest approach was proposed. In this method, a threshold Q_t is used to select similar patches before the filtering. The weight of each selected patch is then defined as

$$W = \exp\left(-\frac{Q}{Q_t}\right) \tag{5}$$

where Q is the sum of the polarimetric similarity between each pair of corresponding pixels in the two noisy patches, which is calculated by the likelihood-ratio test method based on the complex Wishart distribution [24]. Empirically, Q_t is set as

$$Q_t = -\sqrt{k/L} \times n \tag{6}$$

where k is the tuning parameter, and n is the number of pixels in a patch.

b) Improved NLM-based methods: Compared with most of the traditional filters, the pretest NLM filter obtains a good balance in reducing speckle and preserving the spatial resolution of images. Since its introduction, filters based on NLM have been widely studied for PolSAR despeckling. In [30], a method based on the pretest NLM and distributed Lee filter was investigated, in which a kind of hybrid patch similarity measure is constructed by combining the structure similarity introduced by the NLM filter and the homogeneity similarity introduced by the Lee filter, which works in a distributive way. In [31], a new PolSAR NLM filter under the Bayesian framework was proposed, which separately deals with the speckle and the underlying speckle-free signal of the PolSAR data. In [32], Deledalle *et al.* proposed a unified nonlocal framework for the despeckling of amplitude, polarimetric SAR, and/or interferometric SAR images. In general, the studies of PolSAR NLM filters usually concentrate on two main issues: 1) whether or not to select similar patches or how to select similar patches; and 2) how to measure the similarity between patches and thus better calculate the weights. Although the PolSAR NLM filters have shown successful filtering performances, the algorithms' complexity and computational load introduced by the target patch and large search area can be prohibitive for the large datasets (which can have a dimension of more than 10 000 $\times$ 10 000 pixels) from the new space-borne SAR systems, even with the current fast computers.

3) PDE-Based Methods: The denoising methods based on PDEs have been very successful in Gaussian noise removal and have proven their efficiency in filtering images while preserving important data discontinuities that often contain edge information. In recent years, PDE-based methods have also been extended to reduce the speckle in PolSAR images and have shown promising performances.

a) PolSAR anisotropic diffusion (AD) filters: One of the first PDE-based denoising algorithms was the pioneering work of Perona and Malik [22] (the PM model), who developed an AD reconstruction method to smooth gray-valued images while preserving the edges. The basic idea behind AD is to evolve from an original image u^0 and to increasingly smooth the image according to the solution of the following PDE:

$$\frac{du}{dt} = \mathrm{div}[G(|\nabla u|) \cdot \nabla u] \tag{7}$$

where ∇ is the gradient operator, $\mathrm{div}(\cdot)$ is the divergence operator, and $|\cdot|$ denotes the magnitude. $G(\cdot)$ is the diffusion coefficient to ensure that the filtering process diffuses more in smooth areas and less around high-intensity transitions.

In [23], based on the PolSAR filtering principles and the eight-neighborhood discrete scheme of the PM model, the authors proposed a PolSAR AD model

$$\mathbf{C}_x^{t+\Delta t} = \mathbf{C}_x^t + \frac{\Delta t}{8} \sum_{p \in \mathrm{Z}} G(D(\mathbf{C}_x^t, \mathbf{C}_p^t))(\mathbf{C}_p^t - \mathbf{C}_x^t) \tag{8}$$

where Z denotes the set of the eight neighborhoods of pixel x, and Δt is the iteration step, which is often fixed as 0.05. The diffusion process is recursive over time until it meets the stopping criterion. In this model, the same diffusion coefficient constructed by the PolSAR image gradient $D(\mathbf{C}_x^t, \mathbf{C}_p^t)$ is used to filter each term of $\mathbf{C}$ independently and equally, where $D(\mathbf{C}_x^t, \mathbf{C}_p^t)$ is calculated based on Conradsen's hypothesis test [24].

Although the PolSAR AD method can effectively suppress the speckle, notable oversmoothing can sometimes be observed in the processed images. The main reason for this is that, as the diffusion proceeds, the statistical distribution of the data can change, and the original way of calculating the diffusion coefficient becomes inappropriate. Therefore, in a recent paper [25], the authors proposed an adaptive iteratively refined PolSAR AD (AIR-PAD) filter to alleviate the deficiencies of the original PolSAR AD model.

b) Reaction-diffusion-based filter: Another diffusion-based processing model was proposed in [26], which uses a reaction-diffusion system to simultaneously handle the tasks of PolSAR image filtering and classification. The diffusion term acts to smooth the patches within the image classes and make them more homogeneous by reducing the amount of speckle noise. The reaction term tends to move the pixel values toward the closest representative class, by considering the stochastic distances between the pixels and the class center estimated by training data.

c) Trace-based filter: In [27], Foucher *et al.* developed an iterative PDE filter, which has a form similar to local convolution by oriented Gaussian filters. By using the structure tensor, the shapes of the local Gaussian filters are derived from the local structure information. To construct the structure tensor, the amplitudes of all the covariance matrix terms or coherency matrix terms are taken into account. All the terms of the matrix are then filtered independently and equally.

4) Variational Methods: Most of the traditional image denoising methods use the filtering strategy of processing the pixels one by one, by utilizing information obtained from local pixels. However, these local single-point filters cannot take into account the global information hidden in the images. Variational methods, which were first introduced in [33], are an effective way to employ global regularization information to remove noise in the images. The basic idea behind the variational methods is to construct an energy functional, combining a regularization term with a data fidelity term that enforces smoothness while preserving edges. All the pixels are then collaboratively and simultaneously processed by minimizing the energy functional. Beyond the variational methods, models based on TV regularization [33] have shown their particular attractiveness.

a) PolSAR TV model: In the last few years, some variational methods have been developed for SAR despeckling [34]. However, most of them can only handle the problem of filtering SAR intensity or amplitude images. In [35], Nie *et al.*

innovatively proposed a PolSAR TV model based on the Wishart distribution, which is formulated as follows:

$$\hat{\mathbf{C}} = \underset{\mathbf{C}_i \in H^3_{++}}{\arg\min} \left\{ \sum_{i \in I} [Tr(\mathbf{C}_i^{-1}\mathbf{Z}_i) + \log(|\mathbf{C}_i|)] + \lambda ||\mathbf{C}||_{\mathrm{TV}} \right\} \tag{9}$$

where H^3_{++} denotes the definition domain of the 3×3 Hermitian positive-definite matrix, $\mathbf{Z}$ is the observed matrices, and $\mathbf{C}$ represents the noise-free matrices to be estimated. The first term of the right-hand side is the data-fitting term (fidelity term) derived based on the Wishart distance [52], which is deduced from the Bayesian theory according to the statistical distribution of PolSAR data, and the second term is the TV regularization term, which enforces smoothness. $\lambda > 0$ is a small regularization parameter to control the tradeoff between the goodness of fit of the original speckled image and the smoothing requirement due to the regularization term. Since the model is nonconvex, a convex relaxation iterative algorithm is designed to solve the variational problem, based on the variable splitting and alternating minimization techniques.

b) PolSAR nonlocal TV model: Promising filtering performances for the PolSAR TV method were reported in [35], even when the number of looks is low. However, this method often results in staircase effects in homogeneous regions. To mitigate this drawback, Nie *et al.* [36] recently developed a new model for PolSAR despeckling, which combines the Wishart fidelity term in the original PolSAR TV model with a nonlocal regularization term defined for complex-valued fourth-order tensor data. The experiments described in [36] confirmed the nonlocal PolSAR TV model's improvement with regard to the original PolSAR TV model. However, it should be pointed out that, as the new model involves the computation of nonlocal patches and needs to be iteratively solved, the intensive computational complexity and burden may hinder its usage in practical applications.

5) Machine-Learning-Based Despeckling Methods: Machine learning has been a hot topic in image processing over the last decade. Benefiting from the new thoughts and theories in this area, machine-learning-based despeckling techniques have gradually emerged in recent years. Among them, simulated annealing [18], the optimized Bayesian NLM filter (OBNLM) [37], subspace filtering of the Mueller matrix [38], and the PolSAR filter based on simultaneous sparse coding (SSC) [39] are representative methods.

a) Simulated annealing: The idea of simulated annealing [18] comes from the annealing process of solid materials. This method starts from a high temperature and then randomly searches for a solver in the space of solvers based on a certain strategy, so it can obtain a globally optimal solution rather than a locally optimal solution. Although good speckle-suppression performances have been reported when compared with many of the traditional linear filters, the high computational complexity and the artificial bias limit its further application.

b) Optimized Bayesian NLM filter: In [37], an OBNLM with sigma preselection was proposed. Differing from most of the NLM-based filters, the OBNLM employs a human-intervened process to solve a mixed-integer constrained optimization problem, which is aimed at reducing the noisy image variance and maintaining the mean value of the pixels after filtering under the assistance of the user. Although this method was originally designed for single-channel SAR despeckling, it could easily be applied for PolSAR filtering through multichannel adaption.

c) Subspace filtering of the Mueller matrix: In [38], a filtering method was proposed based on subspace decomposition. In this filter, a parameter space consisting of two orthogonal subspaces—the signal subspace (the normalized Mueller coefficients) and the noise subspace (the entropy)—is first defined, and subspace decomposition is then performed (i.e., principal component analysis). The local polarimetric information is then reconstructed from only the significant principal component analysis coefficients.

d) PolSAR filter based on SSC: Sparse representation, which was first introduced in [40], is one of the state-of-the-art signal processing techniques that has provided a new perspective for image denoising. The main idea behind sparse representation is that a complicated signal can be represented by selecting and linearly combining limited atomic signals. Recently, Xu *et al.* [39] innovatively applied the theory of sparse representation to filter PolSAR images, and successful results were reported. In the PolSAR SSC filter, a nonlocal patch ordering algorithm is developed by extracting sliding patches and organizing them in a regular way, and the ordered patches are filtered by SSC based on a weighted simultaneous orthogonal matching pursuit algorithm. Finally, the filtering results are reconstructed from the filtered patches via inverse permutation and subimage averaging.

As noted in the above review, differing from the local window based filters, many of the recent PolSAR despeckling algorithms have been developed by seeking to utilize information from nonlocal pixels or the global image. Methods that search nonlocally similar patches, such as the pretest NLM filter and the PolSAR SSC filter, can obtain good filtering results for an image containing similar repeated patterns. Simultaneously processing all the pixels by optimizing an energy functional, the variational methods and simulated annealing can exploit the global regularization or statistical information hidden in the image. To sum up, the recent developments in PolSAR filtering have shown the trend evolving from local single-point filtering to nonlocal patch-based or globally collaborative filtering. Furthermore, it should be noted that deep learning theory has attracted wide attention in image processing in the last few years, including image denoising [41]. Although no deep-learning-based SAR filters have been found in the literature to date, the successful application of this theory in PolSAR image classification has a promising future [42], [43]. Therefore, we believe that, in the near future, deep-learning-based PolSAR filters will be a hot topic for PolSAR data processing.

IV. Filtering Assessment Indexes

In general, a good PolSAR despeckling technique should have the following characteristics [44]:

1) speckle reduction in homogeneous areas;

2) scene feature preservation (such as texture, edges, and point targets);
3) radiometric preservation;
4) absence of artifacts.

It is impossible for a single index to assess all the aforementioned features of a filter. Many indexes designed for different purposes have been proposed in the literature, some of which are introduced in the rest of this section.

A. Speckle Reduction

The equivalent number of looks (ENL) is an important indicator to assess the amount of speckle in SAR images; hence, it has been widely used for the assessment of the speckle-suppression performances of filters. For SAR intensity images, the ENL is generally computed as

$$\mathrm{ENL} = 1/\sigma_v^2 \tag{10}$$

where σ_v denotes the coefficient of variation in homogeneous areas. Although it is not difficult for a user to select a homogeneous area in the image, it is nontrivial for a computer. Therefore, automatic and rapid determination of the ENL is sometimes needed. For this purpose, and to take into account fully polarimetric information, some automatic PolSAR ENL estimators have been proposed, including the trace-moment-based estimator and the log-determinant-moment-based estimator [45].

B. Scene Feature Preservation

Preservation of scene features of images, such as edges and strong point targets, is a basic demand when designing PolSAR filters. Since the speckle model does not hold in the presence of persistent scatterers or point targets, a good despeckling filter should not significantly change their values. A strong point target is usually characterized by a cluster of pixels whose reflectivity values are much higher than the mean reflectivity of the surrounding scene. Based on this condition, a target-to-clutter ratio (TCR) was employed in [46], which measures the difference in the intensity ratios between point targets and the surrounding areas before and after despeckling by

$$\mathrm{TCR} = |20\log_{10}\frac{\max_p(I_d)}{\mathrm{mean}_p(I_d)} - 20\log_{10}\frac{\max_p(I_s)}{\mathrm{mean}_p(I_s)}| \tag{11}$$

where I_s and I_d are, respectively, the speckled intensity image and the despeckled intensity image. Subscript p denotes the patch containing a point target, and $\max_p$ and mean_p are computed over the patch.

To assess the capability of a filter in preserving edges, many different indicators have been proposed, which can be categorized into two classes, namely, with reference and without reference. Two typical indicators with references are the figure of merit (FOM) [47] and the edge reconstruction error ($\mathrm{ERR_{edge}}$) [16].

1) *FOM:* The FOM index is formulated as

$$\mathrm{FOM} = \frac{1}{\max(n_d, n_r)}\sum_{i=1}^{n_d}\frac{1}{1+\gamma l_i^2} \tag{12}$$

where n_d and n_r are, respectively, the number of edge pixels in the despeckled image and the clean image, l_i denotes the Euclidean distance between the *i*th edge pixel in the despeckled image and its nearest edge pixel in the clean image, and γ is often set as 1/9. A higher FOM value indicates a better edge-preservation result.

2) ERR_{edge}*:* Differing from FOM, the $\mathrm{ERR_{edge}}$ indicator assesses the edge-preservation capability of a filter by utilizing the fully polarimetric information, which is calculated by

$$\mathrm{ERR_{edge}} = \left[\frac{\sum_{i=1}^{N} f(i)||\mathbf{C}_d(i) - \mathbf{C}_r(i)||_F^2}{9\cdot\sum_{i=1}^{N} f(i)}\right]^{\frac{1}{2}} \tag{13}$$

where N is the total pixel number of the image, $\mathbf{C}_d$ and $\mathbf{C}_r$ denote, respectively, the covariance matrices of the despeckled image and the clean image, and $||\cdot||_F$ is the Frobenius norm. $f(i)$ is set as 1, if pixel i locates on the edge; otherwise, it is set as 0. A lower $\mathrm{ERR_{edge}}$ index value indicates a better edge-preservation result.

The major drawback of the assessment procedure with reference lies in the fact that virtually clean images are used. The simulated images differ from the real PolSAR images, in dynamics, gray-level distribution, spatial correlation, and so on. This procedure cannot work in regions that exhibit multiple and variously oriented edges, or man-made structures. Therefore, indexes without reference have been investigated. Two typical indexes are the despeckling evaluation index (DEI) [48] and the edge-preservation degree based on the ratio of average (EPD-ROA) [35].

1) *DEI:* The DEI is designed based on the ratio between the standard deviation over a small neighborhood and that over a larger neighborhood, which is defined as

$$\mathrm{DEI} = \frac{1}{N}\sum_{i,j}\frac{\min\limits_{|p-i|<s,|q-j|<s}(\mathrm{std}(\mathrm{W}_{p,q}^m))}{\mathrm{std}(\mathrm{W}_{i,j}^s)}, m<s \tag{14}$$

where $\mathrm{W}_{p,q}^m$ denotes the window centered at pixel (p,q) roaming in a neighborhood no greater than $s\times s$, which has the size of $m\times m$ pixels.

2) *EPD-ROA:* The EPD-ROA indicator is given by

$$\text{EPD-ROA} = \frac{\sum_{i=1}^{N}|I_{\mathrm{d1}}(i)/I_{\mathrm{d2}}(i)|}{\sum_{i=1}^{N}|I_{\mathrm{s1}}(i)/I_{\mathrm{s2}}(i)|} \tag{15}$$

where I_{d1} and I_{d2} denote the adjacent pixel values of the despeckled image along the horizontal or vertical direction, respectively. Similarly, I_{s1} and I_{s2} denote the corresponding adjacent pixel values of the speckled image. An EPD-ROA value closer to one indicates a better edge-preservation ability.

C. Radiometric Preservation

Two typical indexes for measuring the radiometric preservation capability of PolSAR filters are the mean of ratio (MOR) and the global reconstruction error ($\mathrm{ERR_{global}}$) [16].

1) *MOR:* For a good filter, the mean intensity value of the homogeneous areas in the image, in particular, should be maintained after filtering. Therefore, a MOR value between the

speckled image and the despeckled image significantly different from one indicates some radiometric distortion.

2) ERI_{global}: $\text{ERI}_{\text{global}}$ is an indicator that needs a reference image, which is given by

$$\text{ERI}_{\text{global}} = \left[\frac{\sum_{i=1}^{N} ||\mathbf{C}_D(i) - \mathbf{C}_r(i)||_F^2}{9N} \right]^{\frac{1}{2}} \tag{16}$$

where the symbols are defined in the same way as ERR_{edge}.

V. Experimental Comparison of PolSAR Filters

In this section, we describe the experiments undertaken with two simulated images (one-look and four-look) and two real PolSAR datasets to compare and analyze some of the state-of-the-art PolSAR filtering techniques. As in the review in Section III, the current PolSAR filters can be generally categorized into five classes, so we chose five filters as the representatives of the different classes: the extended sigma filter [12], the AIR-PAD filter [25], the pretest NLM filter [29], the PolSAR NLTV method [36], and the PolSAR SSC filter [39]. The pretest NLM filter was implemented in PolSARpro v5.0 software; the extended sigma filter was programmed by the authors; and the other methods were implemented by the source codes provided by the authors of the respective papers.

A. Selection of Filtering Parameters

The selection of parameters when applying filters directly influences the filtering performance. Among the five methods, the AIR-PAD filter and the PolSAR SSC filter both have only one parameter that needs to be tuned. The parameter in the AIR-PAD filter is the diffusion time T, which is often set as 15 to 20. A larger T can result in better speckle suppression but worse edge preservation. The AIR-PAD filter with $T = 15$ and $T = 20$ was tested. The parameter that needs to be determined in the PolSAR SSC filter is the ENL value of the speckled image, which can be estimated by the means introduced in Section IV.

For the extended sigma filter, there are two parameters to be tuned, namely, the sigma value ξ for selecting similar pixels, and the filtering window size w_1. A larger sigma value or window size can ensure that more pixels are involved in the filtering to better suppress the speckle, but at the expense of smearing the image. We found that, for most of the cases, the sigma value was better set as 0.8 or 0.9. As to the window size, 7×7 or 9×9 was suitable for most of the cases. Therefore, we chose the following parameter settings to test the extended sigma filter: $\xi = 0.8, w_1 = 7 \times 7$; $\xi = 0.9, w_1 = 7 \times 7$; and $\xi = 0.9, w_1 = 9 \times 9$.

For the NLM-based methods, the sizes of the target patch and the search window are the two parameters that always need to be determined. The search window size w_1 is usually set between 11×11 and 21×21, and the patch size w_2 is usually set between 3×3 and 7×7. Larger search window sizes can include more pixels in the filtering, thus better reducing the speckle, but at the cost of reduced computational efficiency and degrading the spatial resolution of the image. In addition, the threshold parameter k in (6), which is empirically set from 15 to 20, should also be initialized when applying the pretest NLM filter. This threshold not only determines which pixel can be included in the filtering, but it also determines the weight of each pixel. For the test of the pretest NLM filter, we fixed w_1 as 15×15 to make a compromise between reducing speckle and retaining details, and just tuned k and w_2 with the following combinations: $k = 15, w_2 = 3 \times 3$; $k = 15, w_2 = 5 \times 5$; and $k = 20, w_2 = 3 \times 3$.

For the PolSAR NLTV filter, there are several parameters that need to be initialized, including the search window size w_1, the target patch size w_2, the iteration times t, the inertial force parameter β, and the number of selected nearest neighbors in the search area r. Among these parameters, we found that the performance of the PolSAR NLTV filter was quite sensitive to the initialization of β, and different datasets could have quite different appropriate values. Therefore, in practice, for each dataset, we implemented the filtering procedure several times by tuning β to obtain a reasonable result. We also found that good filtering results can be obtained when t is fixed as 60 in most of the cases. Larger values of T can obtain a slightly better result, but at the cost of a heavier computational load. Therefore, we fixed w_1 as 15×15, and just tuned r and w_2 with the following combinations to test the PolSAR NLTV filter: $r = 5, w_2 = 3 \times 3$; $r = 5, w_2 = 5 \times 5$; and $r = 10, w_2 = 3 \times 3$.

B. Experiments With Simulated PolSAR Images

The single-look simulated PolSAR image shown inFig. 2 was used to evaluate the effectiveness of the filters. This image was obtained by the procedure proposed by Lee and Pottier [3], based on the Monte Carlo simulation. The image contains linear and nonlinear edges, small targets, and high returns from a corner reflector. To quantify the performances of the filtering methods, we chose the ENL, TCR, ERR_{edge}, and $\text{ERI}_{\text{global}}$ indicators and report them in Table I. These quantitative assessment values are also presented in the form of spider plots in Fig. 1, in which each axis represents a certain ability of the filter. In the spider plots, all the values are linearly rescaled to $[0, 1]$, based on the best results listed in Table I, and a larger new value indicates a better result. For example, the TCR values are rescaled by the following means:

$$\text{TCR}_{\text{new}} = 5.88/\text{TCR}. \tag{17}$$

The spider plots can visualize the general performance of each method and facilitate the analysis of the impact of each parameter on the filtering results.

1) Extended Sigma Filter: At first sight, the extended sigma filter obtains a positive filtering result. However, the image features are overenhanced. In particular, the point targets and high returns around the corner reflector are smeared to some degree, which indicates that these targets were not detected by the extended sigma filter, and thus not well preserved, as revealed by the TCR values. In the target detection step of the extended sigma filter, only those pixels with intensity values higher than the 98th percentile of all pixels are considered as the potential point targets. This target detection strategy is reasonable for a

TABLE I
QUANTITATIVE ASSESSMENT RESULTS FOR THE SIMULATED IMAGES FILTERED BY THE DIFFERENT METHODS

	Parameter setting	$L=1$				$L=4$			
		ENL	TCR	$\mathbf{ERR}_{\text{edge}}$	$\mathbf{ERR}_{\text{global}}$	ENL	TCR	$\mathbf{ERR}_{\text{edge}}$	$\mathbf{ERR}_{\text{global}}$
Extended sigma	$\xi = 0.8, w_1 = 7 \times 7$(shown in Fig. 2)	20.9	18.85	0.90	0.18	33.6	15.40	0.33	0.09
	$\xi = 0.9, w_1 = 7 \times 7$	21.1	19.17	0.95	0.20	34.2	15.65	0.37	0.09
	$\xi = 0.9, w_1 = 9 \times 9$	22.4	20.44	1.04	0.25	36.0	17.53	0.39	0.10
AIR-PAD	$T = 15$(as shown in Fig. 2)	18.1	6.78	0.77	0.59	83.4	3.33	0.37	0.29
	$T = 20$	20.9	7.02	0.91	0.79	94.0	3.39	0.46	0.38
Pretest NLM	$k = 15, w_2 = 3 \times 3$	34.8	11.12	0.30	0.34	79.9	7.33	0.10	0.23
	$k = 15, w_2 = 5 \times 5$	36.0	14.02	0.42	0.30	81.2	11.24	0.19	0.21
	$k = 20, w_2 = 3 \times 3$(as shown in Fig. 2)	36.5	14.46	0.40	0.21	83.8	12.77	0.18	0.14
PolSAR NLTV	$r = 5, w_2 = 3 \times 3$(as shown in Fig. 2)	15.4	5.88	0.30	0.33	55.3	3.21	0.18	0.21
	$r = 5, w_2 = 5 \times 5$	16.1	6.27	0.41	0.39	57.7	3.88	0.22	0.22
	$r = 10, w_2 = 3 \times 3$	18.7	9.14	0.50	0.42	63.9	4.97	0.30	0.28
PolSAR SSC	/	24.1	6.61	1.02	0.70	67.4	4.01	0.38	0.34

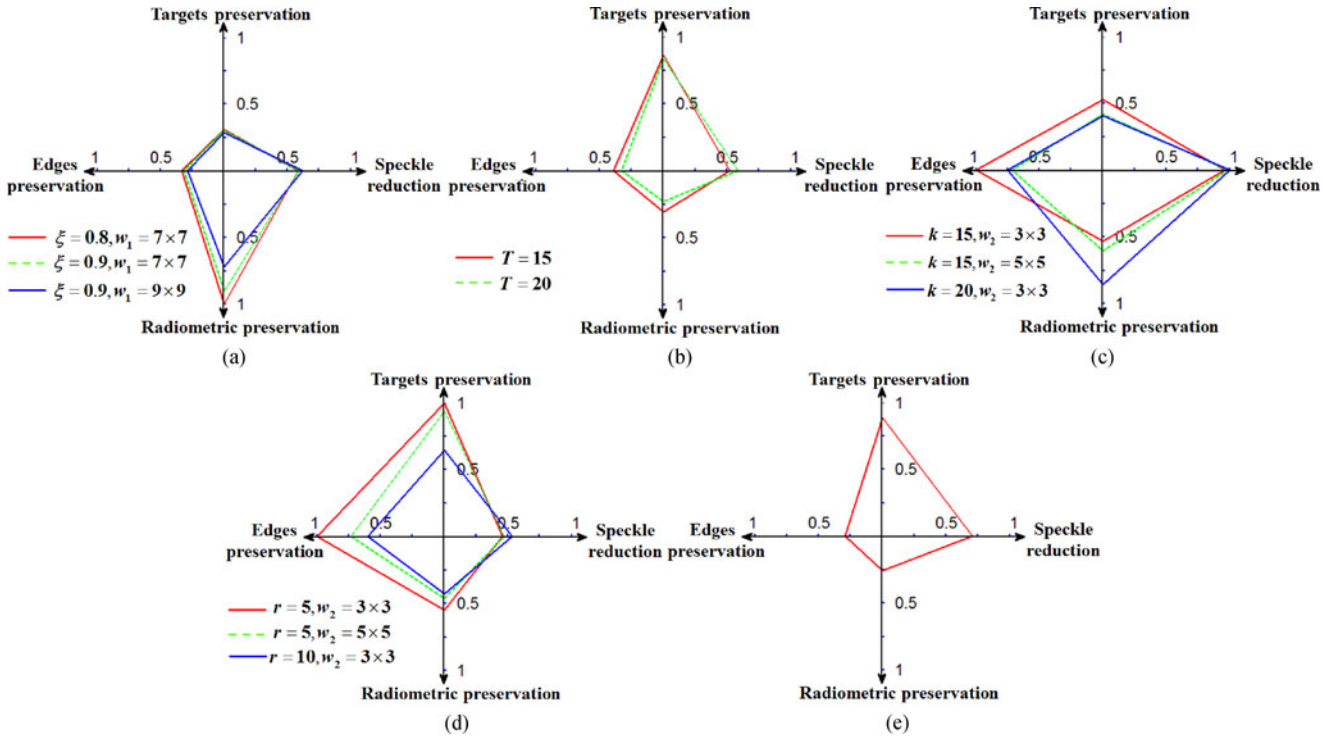

Fig. 1. Spider plots for the one-look simulated image. (a)–(e) Spider plots of the extended sigma filter, the AIR-PAD filter, the pretest NLM filter, the PolSAR NLTV method, and the PolSAR SSC method, respectively.

real scene, since high returns, which often come from point targets, are usually few in a real PolSAR dataset. However, we can observe that the white rectangle in the simulated image dominates the high returns, and thus, the point targets are not successfully detected. There are no distinct differences between the results obtained by different parameter settings, and a general conclusion is that a higher sigma value or a larger filtering window size can better reduce the speckle, but will smear the edges to a greater degree.

2) AIR-PAD Filter: Compared with the extended sigma filter, the AIR-PAD filter shows a better result in preserving point targets. However, we note that a blocky effect is exhibited in the filtered image, which is a common drawback of the AD-based filtering algorithms when processing images with a high level of noise. The blocky effect results in the problem of notable blurring around the edges. This problem is more serious when T is set to 20. As the diffusion proceeds, the image becomes smoother, while the discontinuities around the edges are more

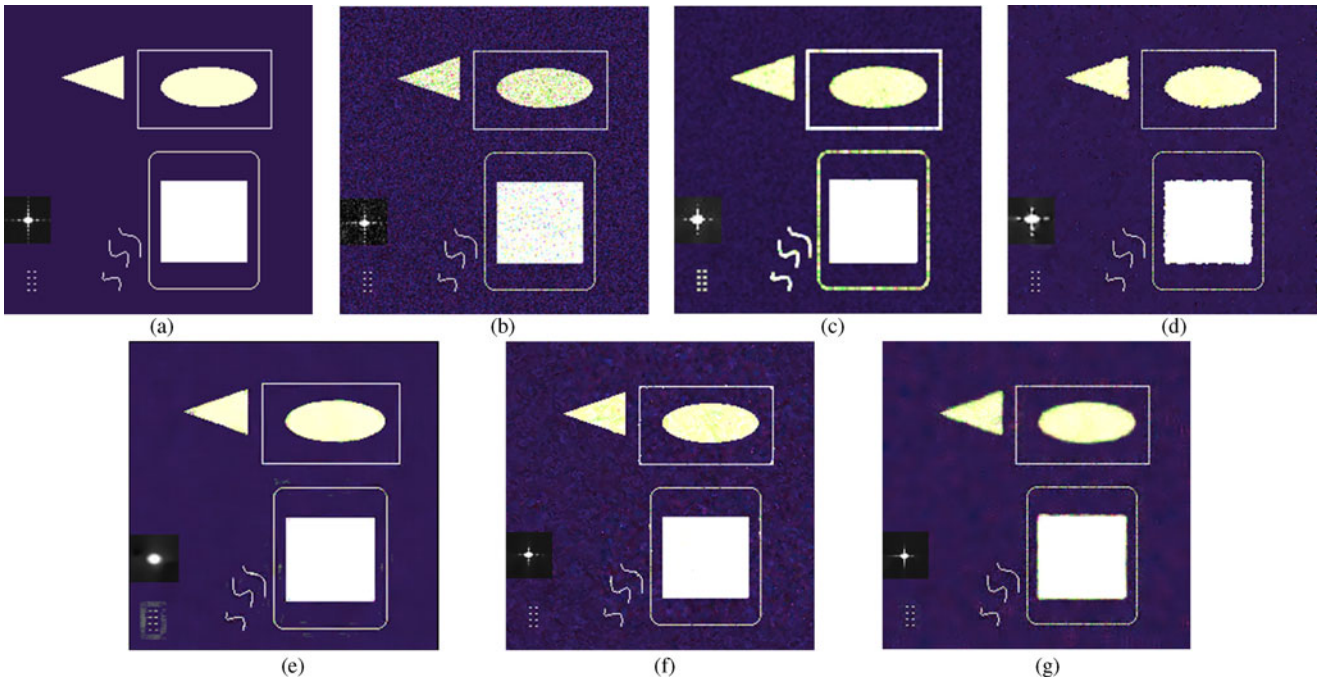

Fig. 2. Filtering results for the single-look simulated image. (a) Noise-free data. (b) Speckled image. (c)–(g) Despeckling results of the extended sigma filter ($\xi = 0.8, w_1 = 7 \times 7$), the AIR-PAD filter ($T = 15$), the pretest NLM filter ($k = 20, w_2 = 3 \times 3$), the PolSAR NLTV method ($r = 5, w_2 = 3 \times 3$), and the PolSAR SSC method, respectively.

inclined to disappear; meanwhile, more radiometric information is lost when T is larger.

3) Pretest NLM Filter: As to the preservation of linear and curved edges, from the visual inspection, the pretest NLM filter [see Fig. 2(e)] undoubtedly obtains quite a good result. This conclusion can also be drawn from the $\mathrm{ERR}_{\mathrm{edge}}$ indicator values listed in Table I. However, a problem brought by this filter is the severe smearing of point signatures, as indicated by the TCR values. Furthermore, we can also observe a phenomenon in that some areas around the point targets and the linear features are "polluted." Parameter k not only determines the weight of each sample, but also determines how many samples can be included in the filtering. A larger k can obtain a better result in suppressing speckle, but a worse result in preserving image details. Furthermore, we found that, for point targets with very few pixels, a smaller target patch size can often obtain a better result in maintaining them. This is because the weight of a patch containing a target is more inclined to be dominated by the similarities between other pixels if the patch is large.

4) PolSAR NLTV Filter: Although the PolSAR NLTV filter obtains good results in retaining the profiles of edges and point targets, it performs quite poorly in reducing speckle. This phenomenon was also noted in [36]. For those images with high levels of speckle, the PolSAR NLTV filter often fails to effectively reduce the speckle. As with the pretest NLM filter, a smaller target patch size in the PolSAR NLTV filter obtains a better result in retaining point targets. As with parameter k in the pretest NLM filter, the number of selected nearest neighbors r in the search area determines how many pixels can be included in the filtering. Therefore, a larger r often results in better speckle suppression, but worse edge preservation.

5) PolSAR SSC Filter: Visually, the PolSAR SSC filter shows a good filtering result. The speckle is effectively suppressed and the features are preserved. However, the filtered image [see Fig. 2(g)] appears oversmoothed and shows a partial halo effect, which directly degrades its performance in radiometric preservation. In practice, although we tried to manually tune and input the ENL value when applying the PolSAR SSC filter, this problem still occurred.

To further validate the capability of the techniques in retaining edges, we show the ratio images in Fig. 3 between the noisy intensity image and the despeckled intensity images. For an ideal filter, the ratio image should be pure speckle. It can be seen that the ratio images for the pretest NLM method and the PolSAR NLTV method have the appearance of random noise, which indicates their good edge-preservation capabilities.

The presence of speckle in a PolSAR image has an impact on the image interpretation. Normally, a good filtering approach can enhance the separation of different land-object classes. To visualize this issue, we plot scattergrams of the Cloude polarimetric decomposition parameters (entropy H, anisotropy A, and alpha angle α) [49] in Fig. 4 for three homogeneous areas of the different images. Clearly, the distributions of the polarimetric decomposition parameters are much more concentrated for the filtered data than for the original data, which verifies the capabilities of the filters in suppressing speckle. However, it should be noted that the distribution of the parameters in the image processed by the PolSAR NLTV method [see Fig. 4(e)] shows a notable shift from the speckled data, which indicates that the PolSAR NLTV filter distorts the polarimetric scattering information of the simulated image, to some degree.

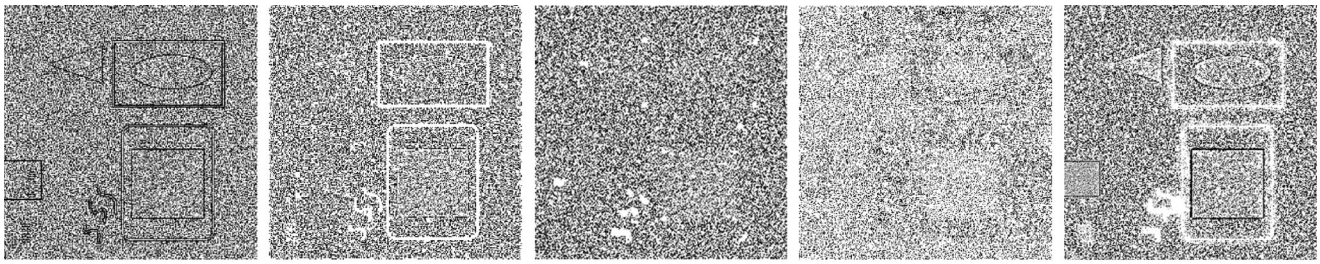

Fig. 3. Ratio images for (a) the extended sigma filter, (b) the AIR-PAD filter, (c) the pretest NLM filter, (d) the PolSAR NLTV filter, and (e) the PolSAR SSC filter.

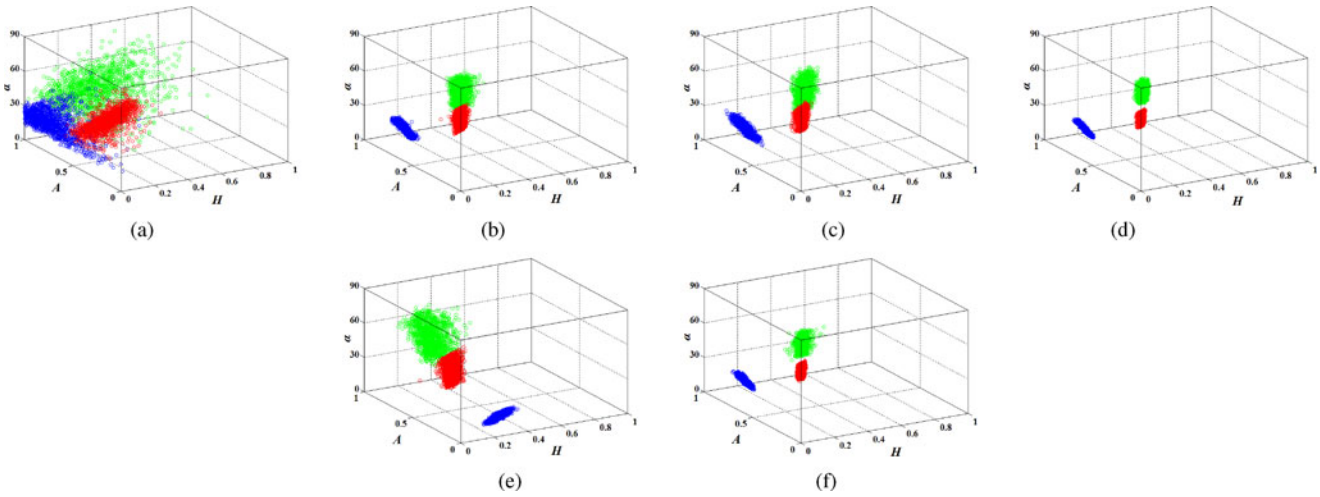

Fig. 4. Scattergrams of the Cloude polarimetric decomposition parameters for different areas in (a) the speckled image and (b)–(f) the images despeckled by the extended sigma filter, the AIR-PAD filter, the pretest NLM filter, the PolSAR NLTV method, and the PolSAR SSC method, respectively.

To compare the methods more objectively, we also list the quantitative assessment results of the five methods on a four-look simulated image in Table I. Generally speaking, most of the conclusions we drew for the single-look speckled image also apply to the four-look image: the pretest NLM filter and the PolSAR NLTV filter perform best in retaining edges, the AIR-PAD filter effectively preserves the targets, and the pretest NLM filter badly smears the targets. However, we can also observe that the performances of the AIR-PAD filter and the PolSAR NLTV filter in reducing speckle are significantly improved as the noise level decreases, and the AIR-PAD filter even obtains the highest value of ENL.

C. Experiments With Two Real PolSAR Datasets

1) Experiments on the San Francisco Dataset: The first real PolSAR dataset used for the comparison of the filtering techniques was the L-band San Francisco dataset, which was acquired by the AIRSAR project of the National Aeronautics and Space Administration/Jet Propulsion Laboratory. This dataset was processed by the European Space Agency as a four-look dataset. To quantitatively evaluate the filtering techniques, we chose the ENL, TCR, EPD-ROA, and MOR indicators, which are reported in Table II. The TCR indicators were obtained by averaging the TCR values for several point targets on the sea, and the MOR indicators were calculated from a homogeneous sea area. The spider plots are shown in Fig. 5, and some of the filtered subimages are displayed in Fig. 6.

As can be observed from Fig. 6, all five filters obtain positive results on the San Francisco image. However, it can be seen that, compared with the other three methods, the extended sigma filter and the PolSAR NLTV filter do not effectively reduce the amount of speckle, especially for the homogeneous ocean area. For these two filters, although expanding the filter window size (enlarging w_1) or including more pixels in the filtering process (enlarging r) can enable them to better reduce the speckle, most of the other performance indexes are degraded, as revealed by the spider plots. Once again, the AIR-PAD filter and the pretest NLM filter reduce the speckle to the greatest degree among the five techniques.

With regard to the preservation of edges, the pretest NLM filter again obtains the best result when parameter k is set to 15. However, enlarging k can degrade the edge-preservation performance. A smaller value of r often obtains a better edge-preservation result for the PolSAR NLTV filter. For the AIR-PAD filter, a better balance between despeckling and retaining details is obtained when T is initialized as 15. From the quantitative evaluation values in Table II and the spider plots, it can be concluded that the PolSAR SSC filter performs the best on this dataset since it obtains quite robust performances in all

TABLE II
QUANTITATIVE ASSESSMENT RESULTS OF THE REAL POLSAR DATASETS FILTERED BY THE DIFFERENT METHODS

	Parameter setting	The San Francisco dataset				The Oberpfaffenhofen dataset			
		ENL	TCR	EPD-ROA	MOR	ENL	TCR	EPD-ROA	MOR
Extended sigma	$\xi = 0.8, w_1 = 7 \times 7$(shown in Figs. 6 and 9)	24.3	2.76	0.758	1.030	14.9	8.57	0.705	1.030
	$\xi = 0.9, w_1 = 7 \times 7$	25.5	2.80	0.750	1.053	15.1	7.45	0.702	1.034
	$\xi = 0.9, w_1 = 9 \times 9$	29.1	8.38	0.742	1.091	16.2	11.42	0.698	1.047
AIR-PAD	$T = 15$(shown in Figs. 6 and 9)	64.2	3.29	0.807	1.003	25.4	14.23	0.684	0.910
	$T = 20$	70.4	5.56	0.788	1.004	32.2	15.45	0.700	0.919
Pretest NLM	$k = 15, w_2 = 3 \times 3$	60.1	3.72	0.841	1.029	29.4	12.57	0.717	0.993
	$k = 15, w_2 = 5 \times 5$	62.4	4.13	0.877	1.001	30.1	13.22	0.702	0.984
	$k = 20, w_2 = 3 \times 3$(shown in Figs. 6 and 9)	66.7	5.21	0.769	1.000	35.0	12.57	0.710	0.986
PolSAR NLTV	$r = 5, w_2 = 3 \times 3$(shown in Figs. 6 and 9)	21.2	3.30	0.824	1.113	10.3	2.77	0.738	0.957
	$r = 5, w_2 = 5 \times 5$	22.1	3.82	0.827	1.139	10.9	2.81	0.730	0.959
	$r = 10, w_2 = 3 \times 3$	29.6	8.71	0.775	0.898	13.3	3.10	0.713	0.948
PolSAR SSC	/	59.1	2.12	0.805	1.030	11.0	7.06	0.709	1.039

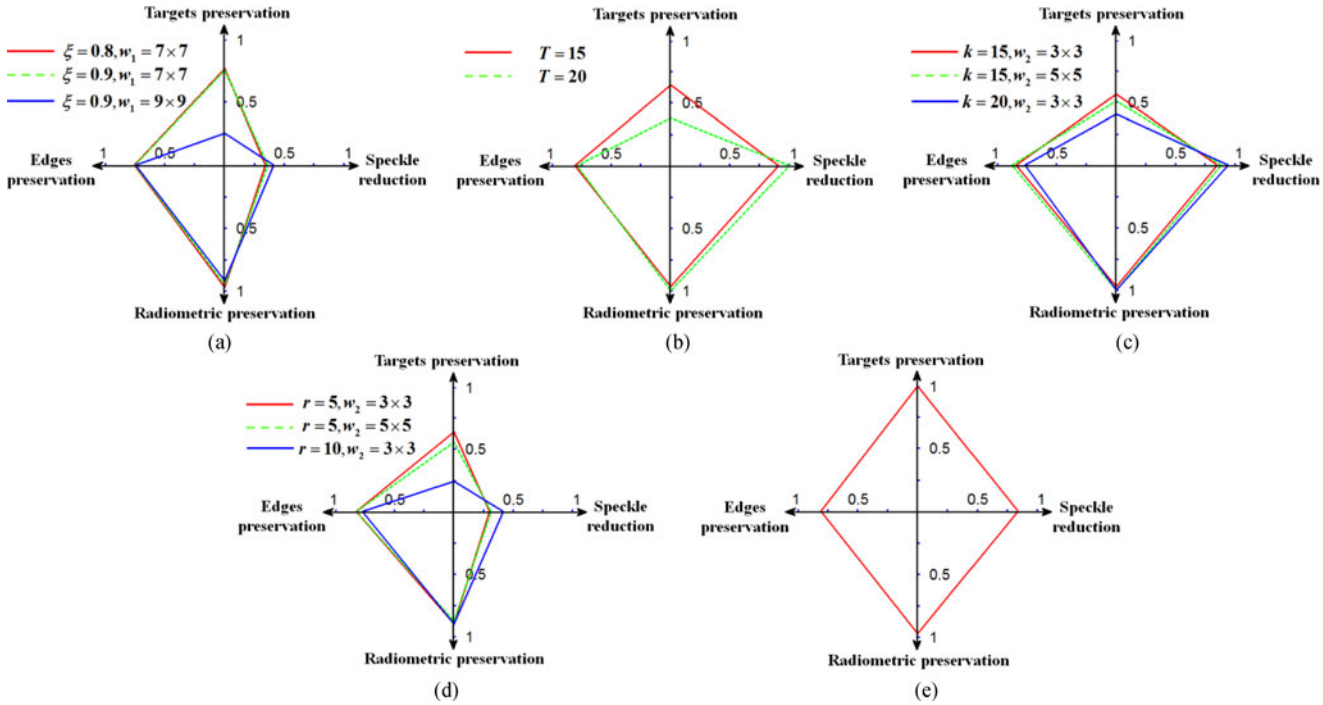

Fig. 5. Spider plots of each filtering technique for the San Francisco dataset. (a)–(e) Spider plots of the extended sigma filter, the AIR-PAD filter, the pretest NLM filter, the PolSAR NLTV method, and the PolSAR SSC method, respectively.

aspects, without distinct drawbacks; however, as observed in the experiments with the simulated images, the PolSAR SSC filtered image again shows a partial halo effect, which slightly degrades the spatial resolution of the image.

Maintaining strong returns from point targets is essential for both target and man-made structure detection. Unlike scattering from distributed media, scattering from point targets comes mainly from a few strong scatterers within a resolution cell, and these targets do not possess the typical characteristics of speckle. It is, therefore, better to maintain their original polarimetric information. In this paper, we use the TCR index to measure the capability of filters in retaining point targets. However, it should be noted that the TCR index can only reflect the difference of the intensity ratios between point targets and the surrounding areas before and after despeckling, and it cannot directly reveal the full polarimetric trait of the target itself. To remedy this deficiency, we chose one of the point targets on the sea, as marked by the arrow in Fig. 6(a) and plotted its cross-polarization signature (see Fig. 7) in each image, as displayed in Fig. 6. The polarimetric signatures, as introduced by Zyl *et al*. [50], plot the normalized copolarization or cross-polarization power density when exploring all the polarization spaces, which can show the amount of power that will be received from a given scatterer for any polarization. Distinct disagreements arise between the signatures from the original pixel and the pixels processed by the pretest NLM filter and the PolSAR NLTV filter, while much

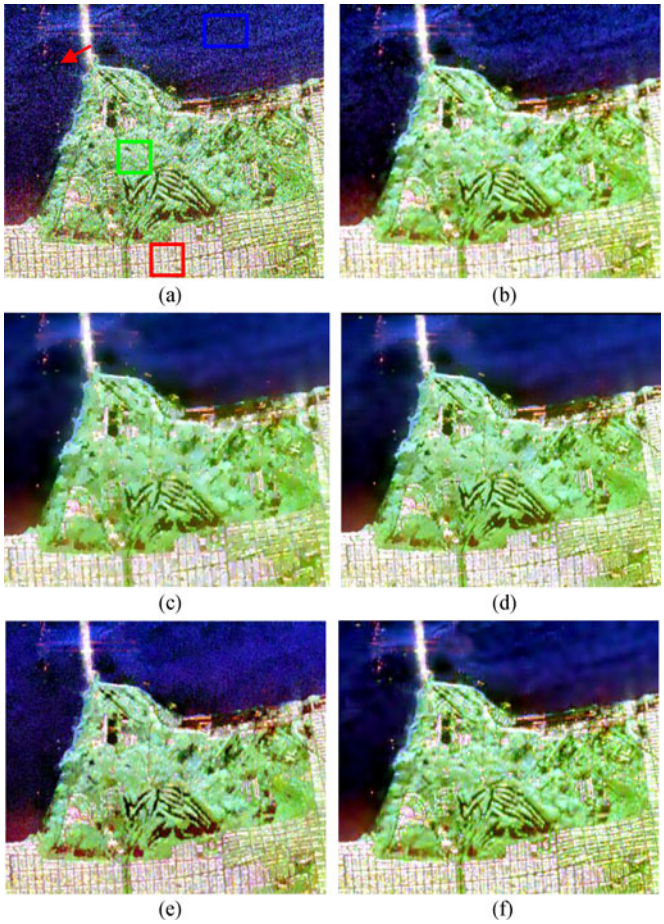

Fig. 6. Filtering results on a subimage of the San Francisco dataset. (a) Pauli RGB image of the speckled data. (b)–(f) Filtering results of the extended sigma filter ($\xi = 0.8, w_1 = 7 \times 7$), the AIR-PAD filter ($T = 15$), the pretest NLM filter ($k = 20, w_2 = 3 \times 3$), the PolSAR NLTV method ($r = 5, w_2 = 3 \times 3$), and the PolSAR SSC method, respectively.

closer agreements are reached for the targets processed by the other techniques. This conclusion is consistent with the one we can draw from the TCR values in Table II, which verifies the validity of the TCR indicator.

To further inspect the capability of the filters in preserving the polarimetric information, we provide scattergrams of the Cloude polarimetric decomposition parameters in Fig. 8 for three areas with different land-object types, as marked in Fig. 6(a). As expected, the objects are much more separable for the filtered data than for the original data, due to the suppression of the speckle. It can also be observed that many sea pixels processed by the PolSAR NLTV method [see Fig. 8(e)] are still very discrete, and some of them even have values of polarimetric anisotropy of nearly 0.5. Anisotropy characterizes the relative magnitudes of the second and third dominant scattering mechanisms. The ocean surface areas have low anisotropy because they are dominated by Bragg scattering, and the other two eigenvalues are random and small in value. In general, after despeckling, the anisotropy is reduced, especially for the low anisotropy areas [13]. Therefore, we can conclude that, as in the experiments on the simulated images, the PolSAR NLTV technique changes the polarimetric scattering mechanisms to some degree. In fact,

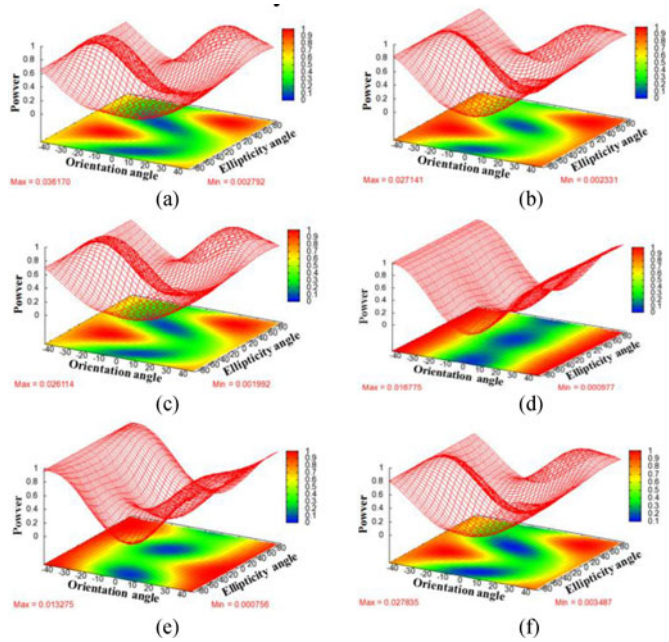

Fig. 7. Comparison of the cross-polarization signatures of a point target in the San Francisco image. (a) Original cross-polarization signatures of the target. (b)–(f) Cross-polarization signatures of the target in the images filtered by the extended sigma filter, the AIR-PAD filter, the pretest NLM filter, the PolSAR NLTV method, and the PolSAR SSC method, respectively.

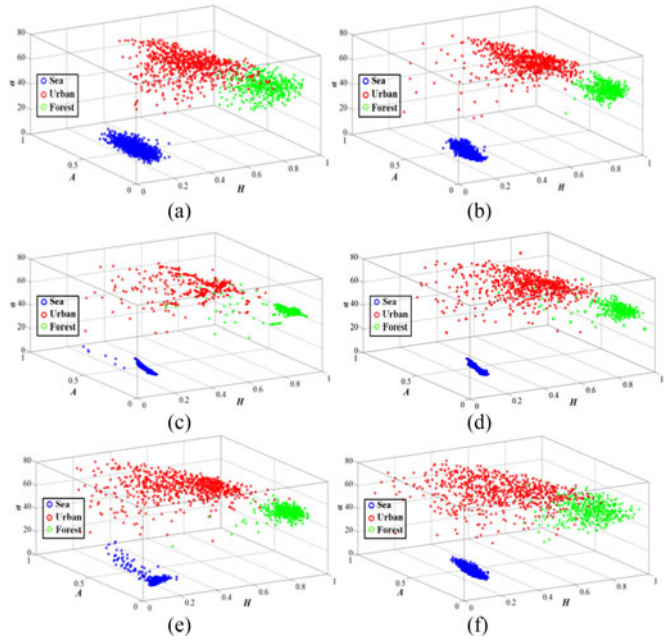

Fig. 8. Scattergrams of the Cloude polarimetric decomposition parameters for different areas in (a) the speckled San Francisco image and (b)–(f) the images despeckled by the extended sigma filter, the AIR-PAD filter, the pretest NLM filter, the PolSAR NLTV method, and the PolSAR SSC method, respectively.

the MOR values calculated on the sea area can also allow this conclusion.

2) Experiments on the Oberpfaffenhofen Dataset: Comparison experiments were also conducted on another real PolSAR dataset, which was a single-look image acquired by the ESAR system over the area of Oberpfaffenhofen airport near Munich.

Fig. 9. Filtering results on two subimages of the Oberpfaffenhofen dataset. (a) Speckled data. (b)–(f) Filtering results of the extended sigma filter ($\xi = 0.8, w_1 = 7 \times 7$), the AIR-PAD filter ($T = 15$), the pretest NLM filter ($k = 20, w_2 = 3 \times 3$), the PolSAR NLTV method ($r = 5, w_2 = 3 \times 3$), and the PolSAR SSC method, respectively.

The filtering results are shown in Fig. 9, and the quantitative evaluation results are reported in Table II.

For this single-look dataset, we found that the diffusion time of the AIR-PAD filter is better set as a larger value, such as 20, to effectively reduce the speckle. However, as the diffusion proceeds, the blocky effect is gradually exhibited in the AIR-PAD filtered image, as found in the experiments with the simulated images. The pretest NLM filter effectively reduces the speckle and enhances the edges; however, the image is slightly oversmoothed and, again, shows the problem of losing some point signatures. Generally speaking, among the five filters, the extended sigma filter, the PolSAR NLTV filter, and the PolSAR SSC filter perform the best in preserving the spatial resolution of the image. In particular, these three techniques retain most of the point signatures. However, it can also be seen that, unlike the good result of suppressing the speckle in the four-look simulated image and the San Francisco image, the PolSAR SSC filter does not effectively reduce the speckle in this severely speckled image. The speckle-suppression capability of the PolSAR NLTV filter is also significantly reduced for this single-look dataset.

In the experiments, we compared five recently developed PolSAR filtering techniques, with both qualitative and quantitative assessments, on two simulated images and two real datasets. To end the experimental part, we provide general descriptions and conclusions for the filtering performance of each method.

1) The extended sigma filter showed a relatively robust filtering performance on all the test images, without distinct drawbacks; however, we found that point targets could be smeared if large distributed targets with high returns existed in the simulated images, which is, of course, rare for real PolSAR images.
2) The AIR-PAD filter obtained positive results in suppressing speckle and maintaining the edge features, particularly in reducing the amount of speckle for the four-look speckled images; however, when the image was badly speckled, a notable blocky effect could be observed in the filtered image.
3) The pretest NLM filter performed well in speckle reduction, edge preservation, and radiometric preservation on all the test images; however, target smearing is its major drawback.
4) The PolSAR NLTV filter obtained very good results in retaining the edge features, even when the speckle level was high. However, the speckle in the images was often not well suppressed compared with the aforementioned filters. In addition, we also found that the PolSAR NLTV

technique could distort the polarimetric scattering information to some degree in certain cases.

5) Among the five filters, the PolSAR SSC filter was the most robust with the four-look images, with good quantitative results in all aspects; however, its capability of reducing speckle was sometimes significantly degraded as the speckle level increased, and some slight artifacts could be observed in the filtered images in many cases.

D. Computational Complexity

In addition to the filtering performance, the computational complexity is also important when assessing the applicability of a despeckling algorithm. For many of the new SAR systems, such as the TerraSAR-X and Cosmo-SkyMed SAR systems, their image dimensions can be as high as 10 000 × 10 000 pixels. Future space-borne SAR systems are expected to have even higher dimensions. Therefore, computationally efficient algorithms will be required for the processing of future PolSAR data. Although it is difficult to directly compare the computational times of the five state-of-the-art methods considered in this paper, since they were implemented on different platforms, we can qualitatively analyze their computational complexity.

First of all, the extended sigma filter is undoubtedly the most computationally efficient method among the five methods, since it is a noniterative local linear filter. For the AIR-PAD filter or the pretest NLM filter, the main computational load comes from the calculation of the similarity between pixels. Although different similarity measures are used in these two methods, by testing, we found that their time costs are close. If we let the size of the image be $m \times n$, the diffusion time be T, and the diffusion step size be Δt, then the complexity of the AIR-PAD filter is about $O_1(8mnT/\Delta t)$; if we let the search window size be $w_1 \times w_1$ and the target patch size be $w_2 \times w_2$, then the complexity of the pretest NLM filter is about $O_1(mnw_1^2 w_2^2)$. Clearly, whether or not the AIR-PAD filter is faster than the pretest NLM filter depends on the selection of the parameters. For the PolSAR NLTV filter, as per the conclusion in [36], the complexity is about $O_2(mnw_1^2 w_2^2 + mnIr)$, where I is the iteration times, r is the number of selected nearest neighbors in the search area, and $O_2(1) \approx O_1(1)$. Clearly, the NLTV filter is less efficient than the pretest NLM filter. For the PolSAR SSC filter, as revealed in [39], the main computational load is the SSC filtering step, which is about 11 times the patch ordering step and takes about 75% of the total time. Assuming that the complexity of calculating the similarity between two pixels in the patch ordering procedure is one step, since the Wishart likelihood-ratio test method [24] is utilized in the patch comparing step, as with the pretest NLM filter, we can deduce that the total computational complexity of the filter is about $O_1[(\lceil \frac{m-w_2}{S} \rceil + 1)(\lceil \frac{n-w_2}{S} \rceil + 1)(\frac{w_1-1}{S})^2 w_2^2] \times 11/0.75$, where $\lceil \cdot \rceil$ is the ceil function and S denotes the sliding step in the patch ordering procedure. We can easily prove that the total computational complexity of the PolSAR SSC filter is slightly lower than the pretest NLM filter, if S is set as 2, as suggested in [39].

VI. Conclusion

In most of the cases, despeckling is an essential procedure for the task of PolSAR image interpretation. In the last three decades, many different PolSAR despeckling algorithms have been proposed. A main goal of this paper was to make a comprehensive review of the existing filtering methods, particularly the recently developed techniques. Generally speaking, the recent developments in PolSAR filtering methods have shown the trend evolving from local single-point filtering to nonlocal patch-based or globally collaborative filtering. Many new filtering methods, especially those methods derived from the idea of NLM, can obtain good results in many cases; however, the high computational burden may hamper their practical application, particularly for the newly launched space-borne PolSAR systems with large image sizes. Furthermore, the fact that several parameters and thresholds need to be tuned is another defect of these methods.

PolSAR image despeckling is an open issue. In a sense, choosing a proper filter is application oriented. To improve the accuracy of land-object classification, it is desirable to choose a filter that can enhance the differences between the classes and preserve the polarimetric scattering mechanisms. To extract strong point targets, such as ships on the sea or man-made structures, one may prefer to choose a filter that can effectively retain high returns. Therefore, it is difficult to directly rate the despeckling methods and evaluate a filter by a single criterion. Many quantitative indexes have been proposed in the literature to assess the filters from different aspects. In this paper, some of these PolSAR despeckling indexes have been introduced and used to compare the performances of five advanced filtering algorithms on two simulated images and two real PolSAR datasets. From the aspect of reducing speckle, retaining details, preserving radiometric information, and avoiding artifacts, we found that most of the state-of-the-art techniques exhibit both strengths and weaknesses. Therefore, in practice, the user needs to choose the filtering method according to the specific demands.

Today, we are on the verge of a new era of operational SAR systems. Recent years have shown a rapid development in advanced PolSAR technology, particularly the availability of high-resolution PolSAR data. On the one hand, recent airborne PolSAR sensors are capable of acquiring images with resolutions down to a few decimeters, together with the all-weather and day-and-night imaging capabilities, making PolSAR a good tool for many applications; on the other hand, these high-resolution PolSAR systems bring new challenges for understanding their speckle statistics, and the feasibility of most of the current PolSAR filters, which were derived based on the assumption of fully developed speckle. Furthermore, as pointed out in [12] and [53], an important question for high-resolution image despeckling is whether or not an intensive filtering procedure needs to be executed. This is because, in the very high resolution PolSAR images, very fine details, such as textures on distributed targets, can emerge; furthermore, the scale of the speckle's granularity in these images becomes much lower than the size of most of the objects to be analyzed. Therefore, in such a case, the speckle effect becomes much less a problem for most image interpretation

tasks, and filters that are able to preserve details and polarimetric information might be a better choice for high-resolution image despeckling.

REFERENCES

[1] C. López-Martínez and X. Fabregas, "Polarimetric SAR speckle noise model," *IEEE Trans. Geosci. Remote Sens.*, vol. 41, no. 10, pp. 2232–2242, Oct. 2003.

[2] S. Foucher and C. López-Martínez, "Analysis, evaluation, and comparison of polarimetric SAR speckle filtering techniques," *IEEE Trans. Image Process.*, vol. 23, no. 4, pp. 1751–1764, Apr. 2014.

[3] J. S. Lee and E. Pottier, *Polarimetric Radar Imaging: From Basics to Applications*. Boca Raton, FL, USA: CRC Press, 2009.

[4] N. Goodman, "Statistical analysis based on a certain multivariate complex Gaussian distribution (an introduction)," *Ann. Math. Statist.*, vol. 34, no. 1, pp. 152–177, 1963.

[5] J. S. Lee, D. L. Schuler, R. H. Lang, and K. J. Ranson, "K distribution for multi-look processed polarimetric SAR imagery," in *Proc. IEEE Geosci. Remote Sens. Symp.*, Pasadena, CA, USA, 1994, pp. 2179–2181.

[6] L. M. Novak and M. C. Burl, "Optimal speckle reduction in polarimetric SAR imagery," *IEEE Trans. Aerosp. Electron. Syst.*, vol. 26, no. 2, pp. 293–305, Mar. 1990.

[7] J. S. Lee, M. R. Grunes, and S. A. Mango, "Speckle reduction in multipolarization, multifrequency SAR imagery," *IEEE Trans. Geosci. Remote Sens.*, vol. 29, no. 4, pp. 535–544, Jul. 1991.

[8] S. Goze and A. Lopes, "A MMSE speckle filter for full resolution SAR polarimetric data," *J. Electromagn. Waves Appl.*, vol. 7, no. 5, pp. 717–737, 1993.

[9] J. S. Lee, M. R. Grunes, and G. D. Grandi, "Polarimetric SAR speckle filtering and its implication for classification," *IEEE Trans. Geosci. Remote Sens.*, vol. 37, no. 5, pp. 2363–2373, Sep. 1999.

[10] J. S. Lee, "A simple speckle smoothing algorithm for synthetic aperture radar images," *IEEE Trans. Syst., Man, Cybern.*, vol. SMC-13, no. 1, pp. 85–89, Jan./Feb. 1983.

[11] J. S. Lee, J. H. Wen, T. L. Ainsworth, K. S. Chen, and A. J. Chen, "Improved sigma filter for speckle filtering of SAR imagery," *IEEE Trans. Geosci. Remote Sens.*, vol. 47, no. 1, pp. 202–213, Jan. 2009.

[12] J. S. Lee, T. L. Ainsworth, Y. Wang, and K. S. Chen, "Polarimetric SAR speckle filtering and the extended sigma filter," *IEEE Trans. Geosci. Remote Sens.*, vol. 53, no. 3, pp. 1150–1160, Mar. 2015.

[13] J. S. Lee, M. R. Grunes, D. L. Schuler, E. Pottier, and L. F. Famil, "Scattering-model-based speckle filtering of polarimetric SAR data," *IEEE Trans. Geosci. Remote Sens.*, vol. 44, no. 1, pp. 176–187, Jan. 2006.

[14] G. Vasile, E. Trouve, J. S. Lee, and V. Buzuloiu, "Intensity-driven adaptive-neighborhood technique for polarimetric and interferometric SAR parameters estimation," *IEEE Trans. Geosci. Remote Sens.*, vol. 44, no. 6, pp. 1609–1621, Jun. 2006.

[15] C. Tomasi and R. Manduchi, "Bilateral filtering for gray and color images," in *Proc. IEEE Int. Conf. Comput. Vision*, 1998, pp. 839–846.

[16] O. D'Hondt, S. Guillaso, and O. Hellwich, "Iterative bilateral filtering of polarimetric SAR data," *IEEE J. Sel. Topics Appl. Earth Observ. Remote Sens.*, vol. 6, no. 3, pp. 1628–1639, Jun. 2013.

[17] C. López-Martínez and X. Fabregas, "Model-based polarimetric SAR speckle filter," *IEEE Trans. Geosci. Remote Sens.*, vol. 46, no. 11, pp. 3894–3907, Nov. 2008.

[18] J. Schou and H. Skriver, "Restoration of polarimetric SAR images using simulated annealing," *IEEE Trans. Geosci. Remote Sens.*, vol. 39, no. 9, pp. 2005–2016, Sep. 2001.

[19] A. Alonso-González, C. López-Martínez, and P. Salembier, "Filtering and segmentation of polarimetric SAR data based on binary partition trees," *IEEE Trans. Geosci. Remote Sens.*, vol. 50, no. 2, pp. 593–605, Feb. 2012.

[20] F. Lang, J. Yang, D. Li, L. Shi, and J. Wei, "Mean-shift-based speckle filtering of polarimetric SAR data," *IEEE Trans. Geosci. Remote Sens.*, vol. 52, no. 7, pp. 4440–4454, Jul. 2014.

[21] B. Pang, S. Xing, Y. Li, and X. Wang, "Novel polarimetric SAR speckle filtering algorithm based on mean shift," *J. Syst. Eng. Electron.*, vol. 24, no. 2, pp. 222–233, 2013.

[22] P. Perona and J. Malik, "Scale-space and edge detection using anisotropic diffusion," *IEEE Trans. Pattern Anal. Mach. Intell.*, vol. 12, no. 7, pp. 629–639, Jul. 1990.

[23] X. Ma, H. Shen, L. Zhang, J. Yang, and H. Zhang, "Adaptive anisotropic diffusion method for polarimetric SAR speckle filtering," *IEEE J. Sel. Topics Appl. Earth Observ. Remote Sens.*, vol. 8, no. 3, pp. 1041–1050, Mar. 2015.

[24] K. Conradsen, A. A. Nielsen, J. Schou, and H. Skriver, "A test statistic in the complex Wishart distribution and its application to change detection in polarimetric SAR data," *IEEE Trans. Geosci. Remote Sens.*, vol. 41, no. 1, pp. 4–19, Jan. 2003.

[25] X. Ma, H. Shen, and L. Zhang, "PolSAR anisotropic diffusion filter with a refined similarity measure and an adaptive fidelity constraint," *Int. J. Remote Sens.*, vol. 37, no. 24, pp. 5988–6011, 2016.

[26] L. Gomez, L. Alvarez, L. Mazorra, and A. C. Frery, "Fully PolSAR image classification using machine learning techniques and reaction-diffusion systems," *Neurocomputing*, vol. 255, no. 13, pp. 52–60, 2017.

[27] S. Foucher, G. Farage, and G. Benie, "Speckle filtering of PoISAR and PolinSAR images using trace-based partial differential equations," in *Proc. Int. Symp. Geosci. Remote Sens.*, 2006, pp. 2545–2548.

[28] A. Buades, B. Coll, and J. M. Morel, "A non-local algorithm for image denoising," in *Proc. IEEE Comput. Soc. Conf. Comput. Vision Pattern Recognit.*, 2005, vol. 2, pp. 60–65.

[29] J. Chen, Y. Chen, W. An, Y. Cui, and J. Yang, "Nonlocal filtering for polarimetric SAR data: A pretest approach," *IEEE Trans. Geosci. Remote Sens.*, vol. 49, no. 5, pp. 1744–1754, May 2011.

[30] H. Zhong, J. Zhang, and G. Liu, "Robust polarimetric SAR despeckling based on nonlocal means and distributed Lee filter," *IEEE Trans. Geosci. Remote Sens.*, vol. 52, no. 7, pp. 4198–4210, Jul. 2014.

[31] G. Liu and H. Zhong, "Nonlocal means filter for polarimetric SAR data despeckling based on discriminative similarity measure," *IEEE Geosci. Remote Sens. Lett.*, vol. 11, no. 2, pp. 514–518, Feb. 2014.

[32] C. A. Deledalle, L. Denis, F. Tupin, A. Reigber, and M. Jager, "NL-SAR: A unified non-local framework for resolution-preserving (Pol)(In)SAR denoising," *IEEE Trans. Geosci. Remote Sens.*, vol. 53, no. 4, pp. 2021–2038, Apr. 2015.

[33] L. I. Rudin, S. Osher, and E. Fatemi, "Nonlinear total variation based noise removal algorithms," *Phys. D: Nonlinear Phenomena*, vol. 60, no. 1, pp. 259–268, 1992.

[34] X. Ma, H. Shen, X. Zhao, and L. Zhang, "SAR image despeckling by the use of variational methods with adaptive nonlocal functionals," *IEEE Trans. Geosci. Remote Sens.*, vol. 54, no. 6, pp. 3421–3434, Jun. 2016.

[35] X. Nie, H. Qiao, and B. Zhang, "A variational model for PolSAR data speckle reduction based on the Wishart distribution," *IEEE Trans. Image Process.*, vol. 24, no. 4, pp. 1209–1222, Apr. 2015.

[36] X. Nie, H. Qiao, B. Zhang, and X. Huang, "A nonlocal TV-based variational method for PolSAR data speckle reduction," *IEEE Trans. Image Process.*, vol. 25, no. 6, pp. 2620–2634, Jun. 2016.

[37] L. Gomez, C. G. Munteanu, M. E. Buemi, J. C. Jacobo-Berlles, and M. E. Mejail, "Supervised constrained optimization of bayesian nonlocal means filter with sigma preselection for despeckling SAR images," *IEEE Trans. Geosci. Remote Sens.*, vol. 51, no. 8, pp. 4563–4575, Aug. 2013.

[38] J. Gu, J. Yang, H. Zhang, Y. Peng, C. Wang, and H. Zhang, "Speckle filtering in polarimetric SAR data based on the subspace decomposition," *IEEE Trans. Geosci. Remote Sens.*, vol. 42, no. 8, pp. 1635–1641, Aug. 2004.

[39] B. Xu, Y. Cui, B. Zuo, J. Yang, and J. Song, "Polarimetric SAR image filtering based on patch ordering and simultaneous sparse coding," *IEEE Trans. Image Process.*, vol. 54, no. 7, pp. 4079–4093, Jul. 2016.

[40] M. Elad and M. Aharon, "Image denoising via sparse and redundant representations over learned dictionaries," *IEEE Trans. Image Process.*, vol. 15, no. 12, pp. 3736–3745, Dec. 2006.

[41] P. Vincent, H. Larochelle, I. Lajoie, Y. Bengio, and P. Manzagol, "Stacked denoising autoencoders: Learning useful representations in a deep network with a local denoising criterion," *J. Mach. Learn. Res.*, vol. 11, pp. 3371–3408, 2010.

[42] Q. Lv, Y. Dou, X. Niu, J. Xu, and B. Li, "Classification of land cover based on deep belief networks using polarimetric RADARSAT-2 data," in *Proc. IEEE Int. Geosci. Remote Sens. Symp.*, 2014, pp. 4679–4682.

[43] L. Jiao and F. Liu, "Wishart deep stacking network for fast POLSAR image classification," *IEEE Trans. Image Process.*, vol. 25, no. 7, pp. 3273–3286, Jul. 2016.

[44] G. D. Martino, M. Poderico, G. Poggi, D. Riccio, and L. Verdoliva, "Benchmarking framework for SAR despeckling," *IEEE Trans. Geosci. Remote Sens.*, vol. 52, no. 3, pp. 1596–1615, Mar. 2014.

[45] S. N. Anfinsen, A. P. Doulgeris, and T. Eltoft, "Estimation of the equivalent number of looks in polarimetric synthetic aperture radar imagery," *IEEE Trans. Geosci. Remote Sens.*, vol. 47, no. 11, pp. 3795–3809, Nov. 2009.

[46] F. Argenti, A. Lapini, and L. Alparone, "A tutorial on speckle reduction in synthetic aperture radar images," *IEEE Geosci. Remote Sens. Mag.*, vol. 1, no. 3, pp. 6–35, Sep. 2013.

[47] W. K. Pratt, *Digital Image Processing*. New York, NY, USA: Wiley-Interscience, 1977.
[48] Y. Zhao, J. Liu, B. Zhang, W. Hong, and Y. Wu, "Adaptive total variation regularization based SAR image despeckling and depeckling evaluation index," *IEEE Trans. Geosci. Remote Sens.*, vol. 53, no. 5, pp. 2765–2774, May 2015.
[49] S. R. Cloude and E. Pottier, "An entropy based classification scheme for land applications of polarimetric SAR," *IEEE Trans. Geosci. Remote Sens.*, vol. 35, no. 1, pp. 68–78, Jan. 1997.
[50] J. J. Zyl, H. A. Zebker, and C. Elachi, "Imaging radar polarization signatures: Theory and observation," *Radio Sci.*, vol. 22, pp. 529–543, 1987.
[51] P. Milanfar, "A tour of modern image filtering, "*IEEE Signal Process. Mag.*, vol. 30, no. 1, pp. 106–128, Jan. 2013.
[52] J. S. Lee, M. R. Grunes, and R. Kwok, "Classification of multi-look polarimetric SAR imagery based on complex Wishart distribution," *Int. J. Remote Sens.*, vol. 15, no. 11, pp. 2299–2311, 1994.
[53] A. Reigber *et al.*, "Very-high-resolution airborne synthetic aperture radar imaging signal processing and applications," *Proc. IEEE*, vol. 101, no. 3, pp. 759–783, Mar. 2013.

Xiaoshuang Ma received the B.S. degree in geographic information system from Hubei University, Wuhan, China, in 2011, and the Ph.D. degree in cartography and geographic Information engineering from Wuhan University, Wuhan, in 2016.

He is currently a Lecturer with the Department of Resources and Environmental Engineering, Anhui University, Hefei, China. His research interests include SAR image processing and interpretation.

Penghai Wu (M'16) received the B.S. degree in environmental science from Anqing Normal College, Anqing, China, in 2009, and the M.S. degree in surveying and mapping engineering and the Ph.D. degree in cartography and geographical information engineering from Wuhan University, Wuhan, China, in 2011 and 2014, respectively.

He is currently an Associated Professor with the School of Resources and Environmental Engineering, Anhui University, Hefei, China. He has authored or coauthored more than 20 research papers, including more than ten peer-reviewed articles in international journals such as the *Remote Sensing of Environment* and the IEEE TRANSACTIONS ON GEOSCIENCE AND REMOTE SENSING. His research interests include spatiotemporal fusion, the reconstruction of land surface temperature, and regional eco-environmental change.

Yanlan Wu received the B.S. degree in engineering surveying and the M.S. degree in engineering surveying from Wuhan Technology University of Survey and Mapping, Wuhan University, Wuhan, China, in 1995 and 1998, respectively, and the Ph.D. degree in cartography and geographic information systems (GIS) from Wuhan University, Wuhan, China, in 2004.

She is currently a "Wan-Jiang Scholar" Distinguished Professor with the School of Resources and Environmental Engineering, Anhui University, Hefei, China. The title of her doctoral dissertation was "Research on Map Algebra Model and Method of 3D Relief Generation." She has authored or coauthored more than 40 research papers since 2001. Her research has been supported by the "863" program, National Natural Science Foundation of China, and other scientific research projects. Her recent research interests have included maritime delimitation technology, digital elevation models, deep learning, and the application of GIS, remote sensing, and global navigation satellite systems in ecology.

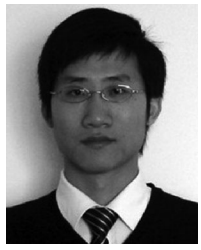

Huanfeng Shen (M'10–SM'13) received the B.S. degree in surveying and mapping engineering and the Ph.D. degree in photogrammetry and remote sensing from Wuhan University, Wuhan, China, in 2002 and 2007, respectively.

In 2007, he joined the School of Resource and Environmental Sciences, Wuhan University, where he is currently a Luojia Distinguished Professor. He has authored more than 100 research papers. His research has been supported by several talent programs, such as the Youth Talent Support Program of China (2015), the China National Science Fund for Excellent Young Scholars (2014), and the New Century Excellent Talents by the Ministry of Education of China (2011). His research interests include image quality improvement, remote-sensing mapping and application, data fusion and assimilation, and regional and global environmental change.

Dr. Shen is a member of the Editorial Board of the *Journal of Applied Remote Sensing*.